

---

[All ETDs from UAB](#)

[UAB Theses & Dissertations](#)

---

2006

## Change In Conduction Velocity Due To 2D Fiber Curvature In Cultured Neonatal Rat Ventricular Myocytes

Elliot Blake Bourgeois  
*University of Alabama at Birmingham*

Follow this and additional works at: <https://digitalcommons.library.uab.edu/etd-collection>



Part of the [Engineering Commons](#)

---

### Recommended Citation

Bourgeois, Elliot Blake, "Change In Conduction Velocity Due To 2D Fiber Curvature In Cultured Neonatal Rat Ventricular Myocytes" (2006). *All ETDs from UAB*. 3558.  
<https://digitalcommons.library.uab.edu/etd-collection/3558>

This content has been accepted for inclusion by an authorized administrator of the UAB Digital Commons, and is provided as a free open access item. All inquiries regarding this item or the UAB Digital Commons should be directed to the [UAB Libraries Office of Scholarly Communication](#).

CHANGE IN CONDUCTION VELOCITY DUE TO 2D FIBER CURVATURE IN  
CULTURED NEONATAL RAT VENTRICULAR MYOCYTES

by

ELLIOT BLAKE BOURGEOIS

JACK M. ROGERS, COMMITTEE CHAIR  
VLADIMIR G. FAST  
GREGORY P. WALCOTT

A THESIS

Submitted to the graduate faculty of The University of Alabama at Birmingham,  
in partial fulfillment of the requirements for the degree of  
Master of Science in Biomedical Engineering

BIRMINGHAM, ALABAMA

2006

# CHANGE IN CONDUCTION VELOCITY DUE TO 2D FIBER CURVATURE IN CULTURED NEONATAL RAT VENTRICULAR MYOCYTES

ELLIOT BLAKE BOURGEOIS

## ABSTRACT

Continuum modeling of two-dimensional curved fiber fields has suggested that fiber curvature modulates conduction velocity (CV) in the myocardium. To verify the existence of this effect in living tissue, we measured CV in macroscopically anisotropic monolayers of cultured neonatal rat ventricular myocytes with controlled fiber curvature. A novel growth-directing substrate was used to produce fiber fields with significant curvature ( $78^{\circ}/\text{cm}$  to  $333^{\circ}/\text{cm}$ ). Anisotropy ratios (longitudinal CV / transverse CV) measured in cultures grown using this method ( $n=32$ ) were  $2.3 \pm 0.3$ , which is similar to the anisotropy exhibited by human ventricular myocardium. Propagating wavefronts were initiated transverse to fiber orientation in two alternating directions (with respect to fiber curvature) using unipolar stimulation. Action potentials were recorded using a voltage-sensitive fluorescent dye (di-4-ANEPPS) and a high speed digital video camera. A statistically significant ( $p=0.00033$ ) change in CV was observed when propagation direction was reversed with respect to the direction of fiber curvature. The measured change in CV was  $0.38 \pm 0.44$  cm/s for all samples ( $n=24$ ). A control group of cultures with uncurved transverse fiber orientation was also studied, and a  $0.06 \pm 0.18$  cm/s ( $p=\text{NS}$ ) difference in CV was measured for propagation in both directions in this group ( $n=8$ ). We conclude that fiber curvature can affect CV and may be involved in arrhythmogenesis, for example, by promoting wavebreak or conduction block.

## DEDICATION

To my parents and my sister for their encouragement and support, to Jack Rogers for always inspiring good science and for funding this work, and to the Little Lebowski Urban Achievers (“and proud we are of all of them”).

## TABLE OF CONTENTS

	<i>Page</i>
ABSTRACT.....	ii
DEDICATION.....	iii
LIST OF FIGURES .....	v
INTRODUCTION .....	1
Background and Significance .....	1
Specific Aims.....	4
CHANGE IN CONDUCTION VELOCITY DUE TO 2D FIBER CURVATURE IN CULTURED NEONATAL RAT VENTRICULAR MYOCYTES .....	6
CONCLUSIONS.....	28
LIST OF REFERENCES.....	29
APPENDIX: IACUC ANIMAL USE APPROVAL FORM .....	32

## LIST OF FIGURES

<i>Figure</i>	<i>Page</i>
1 Geometry of growth directing substrates.....	22
2 Geometry of perfusion bath with electrodes.....	23
3 Method for conduction velocity calculation .....	24
4 Myofibril curvature as resolved by fluorescent actin filament staining .....	25
5 Average conduction velocities for all curved fiber samples.....	26
6 Two dimensional propagation across curved fibers of anisotropic cells .....	27

## INTRODUCTION

### **Background and Significance**

Coronary heart disease has been the most common cause of death in the United States for over 50 years, and is currently responsible for nearly 700,000 deaths per year.<sup>1</sup> Sudden cardiac death (SCD) accounts for about half of these cases.<sup>1-3</sup> SCD often occurs without presenting any symptoms before the lethal episode; predisposition for SCD is difficult to identify, and current preemptive treatments for SCD are inadequate.<sup>2,3</sup>

The normal electrical activity of the heart must be disrupted for SCD to occur. Numerous pathologies can contribute to the initiation and proliferation of arrhythmic events. These factors include congenital diseases (long-QT syndrome, Wolff-Parkinson-White syndrome, Brugada's syndrome, idiopathic ventricular fibrillation), anatomical deformations (coronary artery disease, hypertrophy, ventricular dysplasia, interstitial fibrosis), transient events (ischemia, sudden physical activity, stress, electrolytic fluctuations, exposure to drugs, neurotransmitters and hormones), and basic arrhythmic mechanisms (reentry, automaticity, triggered activity, cell-to-cell uncoupling and conduction block).<sup>2</sup> Arrhythmogenesis typically involves the interplay of several of these conditions, so predicting the circumstances that will lead a particular heart into arrhythmia is difficult.

Most SCDs are attributed to ventricular fibrillation (VF), a fast arrhythmia that prevents the heart from pumping blood.<sup>4</sup> The complex wave patterns observed during VF result when a simpler arrhythmia, such as a spiral wave, encounters heterogeneities in the

tissue that cause the wave to fragment. A normal conduction pattern can traverse small obstacles unaffected because a normal wavefront is wide enough to absorb small scale variances; however, faster moving wavefronts, like those emanating from reentrant circuits, have a narrower width and are more susceptible to alteration by tissue anomalies.<sup>5</sup> Heterogeneous regions are defined as localized irregularities in excitability and conduction velocity (CV),<sup>6</sup> and can result from any number of pathologies (as described above) or from local variances in temporal factors, such as refractoriness.<sup>7</sup> It has been proposed that complexities in the geometry of the heart can constitute tissue heterogeneities capable of inducing wavebreak or conduction block, even in otherwise homogeneous tissue.<sup>8,9</sup>

A simple reentrant wavefront, such as a spiral wave, can quickly evolve into VF upon encountering heterogeneous regions of tissue. Spiral waves begin to drift when they either rotate fast enough so that they encounter their own refractory tail,<sup>10</sup> or they encounter inhomogeneous media that change the path of the wavetip.<sup>11</sup> Simulations have shown that three dimensional surface curvature can induce spiral waves to meander even if the medium is homogeneous,<sup>9</sup> and fiber curvature alone has caused spiral waves to drift in two dimensional simulations.<sup>8</sup>

Waves emanating from a nonstationary spiral wave source have variable periodicity as a result of the Doppler effect; waves moving in the same direction as the spiral wave source have a higher frequency than waves moving in the opposite direction of the source.<sup>12</sup> This phenomenon increases the likelihood that the wavefront will fragment: the frequency of stimulation is increased in the direction of spiral drift, and propagation will block if the tissue is overdriven (and thus refractory). Neighboring



tissues not directly along the axis of spiral drift will be driven at a slower rate, and the closeness of this discrepancy in refractoriness can provide an avenue for the overdriven impulse to break into multiple wavelets.<sup>4</sup>

Ventricular geometries have been measured for dog,<sup>13</sup> rabbit,<sup>14</sup> and pig.<sup>15</sup> Numerous macroscale invaginations and protuberances are prevalent in the ventricular endocardium (trabeculae, papillary muscles) of all these models. Anisotropic fiber orientation is largely consistent in all models, with a transmural rotation in fiber angle from epicardium to endocardium of up to 140°; fiber curvature is also observed in two dimensions within each layer of fibers in the myocardium.<sup>13-15</sup> Complex surface geometries exist in the atrial endocardium as well (pectinate muscles).<sup>16,17</sup>

Ventricular trabeculae and the insertion points of papillary muscles have been shown to provide stable physical centers for wavebreak and reentry.<sup>18</sup> YH Kim, et al. showed that spiral waves often anchor to the insertion point of a papillary muscle in an isolated right ventricle, and after the papillary muscles were shaved off at the level of the endocardium, sustained ventricular tachycardia (VT) could no longer be induced.<sup>19</sup> There is potential for a variety of curved fiber scenarios at the papillary muscle, as the number, structure, and location of the papillary muscles vary widely from one heart to another.<sup>20</sup>

By mapping the wave fronts in cell cultures with two dimensional fiber curvature, areas of significant fiber curvature can be identified as possible instigators of wave break or conduction block. While wavebreak, conduction block, and reentry have frequently been observed to occur in regions of sharp fiber curvature in whole heart studies, it cannot be concluded that fiber curvature is exclusively responsible for these effects,

because curvature geometries are not consistent from one heart to another, and a multitude of complicating structural variances (blood vessels, connective tissues, Purkinje fibers) exist in living myocardium.

Cell culture studies have been used to demonstrate geometric effects of boundaries<sup>21-23</sup> and rapid changes in cable width,<sup>24</sup> and confluent anisotropic sheets of cells with straight-line fiber orientation have been achieved in cell culture.<sup>25,26</sup> CV in these cultures is anisotropic and mimics CV observed in vivo, favoring longitudinal over transverse propagation. Curved fiber anisotropy has not yet been demonstrated, but existing methods<sup>25</sup> can be modified to achieve this with minimal difficulty.

The magnitude of fiber curvature can be quantified using a vector,  $\kappa$ :

$$\kappa = \frac{\partial \phi}{\partial s} = \frac{1}{r} \quad [1]$$

where  $\phi$  is the tangential angle,  $s$  is the arc length, and  $r$  is the radius of curvature. Simulations have shown that  $\kappa = 15^\circ/\text{cm}$  is sufficient to observe a change in CV when propagation in the direction of the curvature vector is compared to propagation in the opposite direction of the curvature vector.<sup>8</sup> A fiber curvature of at least this value will be used in this study to verify the effect of fiber curvature on CV.

### **Specific Aim**

Monolayers with controlled fiber curvature were used in this study to measure CV when waves propagate in the same direction of the fiber curvature vector, and to measure CV when waves propagate in the opposite direction of the fiber curvature vector. Although sites of significant fiber curvature may influence CV changes it is difficult to test for this effect in myocardium because of the complex, heterogeneous, three

dimensional nature of the tissue. Monolayers of cardiac myocytes are an ideal preparation for testing for this effect because they are two dimensional, fiber curvature can be controlled, and other heterogeneities, while present, are randomly distributed. Anisotropy in cell culture was produced by scratching the growing substrate in a manner similar to the method used by Bursac, et al.<sup>25</sup> Anisotropy was verified by fluorescent actin staining.<sup>27</sup>

Unipolar stimulating electrodes were used to initiate wavefront propagation in the cell cultures. Switching between the two electrodes allowed alternation between propagation in the same direction as, and in the opposite direction as, the fiber curvature vector. Optical mapping was used to detect propagating waves in the monolayer.

CHANGE IN CONDUCTION VELOCITY DUE TO 2D FIBER CURVATURE IN  
CULTURED NEONATAL RAT VENTRICULAR MYOCYTES

by

ELLIOT B. BOURGEOIS, VLADIMIR G. FAST, REUBIN L. COLLINS,  
JAMES D. GLADDEN, JACK M. ROGERS

Submitted to *Circulation Research*

Format adapted for thesis

### Abstract

Continuum modeling of two-dimensional curved fiber fields has suggested that fiber curvature modulates conduction velocity (CV) in the myocardium. To verify the existence of this effect in living tissue, we measured CV in macroscopically anisotropic monolayers of cultured neonatal rat ventricular myocytes with controlled fiber curvature. A novel growth-directing substrate was used to produce fiber fields with significant curvature ( $78^{\circ}/\text{cm}$  to  $333^{\circ}/\text{cm}$ ). Anisotropy ratios (longitudinal CV / transverse CV) measured in cultures grown using this method ( $n=32$ ) were  $2.3 \pm 0.3$ , which is similar to the anisotropy exhibited by human ventricular myocardium. Propagating wavefronts were initiated transverse to fiber orientation in two alternating directions (with respect to fiber curvature) using unipolar stimulation. Action potentials were recorded using a voltage-sensitive fluorescent dye (di-4-ANEPPS) and a high speed digital video camera. A statistically significant ( $p=0.00033$ ) change in CV was observed when propagation direction was reversed with respect to the direction of fiber curvature. The measured change in CV was  $0.38 \pm 0.44$  cm/s for all samples ( $n=24$ ). A control group of cultures with uncurved transverse fiber orientation was also studied, and a  $0.06 \pm 0.18$  cm/s ( $p=\text{NS}$ ) difference in CV was measured for propagation in both directions in this group ( $n=8$ ). We conclude that fiber curvature can affect CV and may be involved in arrhythmogenesis, for example, by promoting wavebreak or conduction block.

## Introduction

Anatomical and electrical anisotropy are properties of all cardiac muscle, and are necessary for the heart to function. Individual cardiac cells form elongated cylindrical geometries that align axially along cardiac fibers,<sup>1,2</sup> and directional fiber orientation engenders macroscopic anatomical anisotropy throughout the heart. Intercellular connectivity is also anisotropic—gap junctions (the primary pathway for intercellular ionic currents) are predominantly found at the ends of the long axis of the myocyte (the longitudinal direction), while comparatively few gap junctions are found between the sides of adjacent cells (the transverse direction).<sup>2,3</sup> Electrical anisotropy results from these directional configurations—transverse intercellular resistance is higher than longitudinal intercellular resistance, resulting in slower wave propagation velocity in the transverse direction.<sup>4-6</sup>

Anisotropic excitation and propagation behaviors that result from fiber directionality become more complex when fibers are curved. A better understanding of the nature of fiber curvature effects will yield a more complete picture of conduction in the heart. The magnitude of fiber curvature can be quantified by the curvature of a line tracing the longitudinal axis of the fibers. Curvature is represented with a vector,  $\kappa$ , drawn perpendicular to the local fiber orientation and pointing in the direction of the center of curvature. The magnitude of  $\kappa$  is the inverse of the radius of curvature. When the fibers are not curved, the magnitude of  $\kappa$  is zero, and propagation is the same in both possible transverse directions. However, for nonzero  $\kappa$ , computer modeling has shown that CV is reduced, relative to the straight fiber case, when transverse waves propagate in the same direction as  $\kappa$  (Transverse With, or TW, propagation); conversely, CV is

increased when waves propagate in the opposite direction of  $\kappa$  (Transverse Against, or TA, propagation).<sup>7</sup> These effects are due to differential current loading at the wavefront in both cases.

Fiber geometries have been measured in dog,<sup>8</sup> rabbit,<sup>9</sup> and pig<sup>10</sup> hearts. Anisotropic fiber orientation is largely consistent in all models, with a transmural rotation in fiber angle from epicardium to endocardium of up to 140°. Fiber curvature is observed in two dimensions within each layer of fibers in the myocardium.<sup>8-10</sup> Numerous macroscale invaginations and protuberances are found in the ventricular endocardium (trabeculae, papillary muscles) of all hearts, which likely results in complex fiber curvatures where such structures join the bulk myocardium. Ventricular trabeculae and the insertion points of papillary muscles have been shown to provide stable physical centers for wavebreak and reentry.<sup>11</sup> YH Kim, et al. showed that spiral waves often anchor to the insertion point of a papillary muscle in an isolated right ventricle, and after the papillary muscles were shaved off at the level of the endocardium, sustained ventricular tachycardia (VT) could no longer be induced.<sup>12</sup> Complex geometries exist in the atrial endocardium as well (pectinate muscles), and it has been proposed that these geometries can exacerbate arrhythmogenesis.<sup>13,14</sup> These effects are not yet well understood, but may involve fiber curvature.

The effect of fiber curvature has been clearly demonstrated in computer models.<sup>7</sup> However, the heterogeneous nature of native tissue preparations makes it difficult to experimentally isolate fiber curvature's role from that of other heterogeneities. Macroscale anisotropy in cell culture has recently been achieved,<sup>5,6</sup> and we have produced curved fiber fields on a macroscopic scale using a similar method. In the

present study, we use this preparation to demonstrate the effect of fiber curvature on cardiac propagation velocity in an otherwise homogeneous medium.

## **Materials and Methods**

### *Substrate Preparation*

Polyvinyl chloride (PVC) coverslips (Fischer Scientific) were scratched using a razor blade with a micro-scale serrated edge. Controlled serrations were made in the edge of the razor blade using a fly-cutter on a tabletop milling machine (Sherline Model 2000). Milling feed and speed were adjusted to produce serrations at 18 $\mu$ m spacing, consistent with the width of scratches previously shown<sup>5</sup> to maximize anisotropy. The serrated blade was then secured in the chuck of the milling machine and PVC coverslips were mounted on a rotary table to allow scratches to be made in a controlled arc. Straight scratches were produced above and below the region of curved scratches to maintain transverse propagation throughout the culture. Two rectangular holes were punched in the coverslip to create boundaries around the region of curved scratches. These boundary conditions helped to maintain approximately transverse wavefronts in the resulting channel of curved fibers (Figure 1). To remove any machining residues, coverslips were sonicated in a solution containing Alconox detergent powder (VWR Scientific) for 30 minutes and thoroughly washed with deionized water. The substrates were then gas sterilized.



### *Cell Culture*

Ventricular myocytes were obtained from two to three day old Sprague-Dawley rats (Harlan) using a method previously described,<sup>15</sup> with the following modifications: UltraCulture cell medium (BioWhittaker) was used instead of medium M199. High serum medium and normal serum medium are now the same medium, containing 6.67% fetal bovine serum. To permit cell adhesion, substrates were coated with collagen (extracellular matrix protein collagen type IV from human placenta, Sigma) dissolved in a phosphate buffer at a concentration of 100 ug/mL. Measurements were made on days 4-6 of culture to maximize cell growth and monolayer confluence.

### *Optical Mapping*

Voltage-sensitive dye (di-4-ANEPPS, Invitrogen) was used to optically detect cell depolarization, and data were recorded at 1000 frames per second with a CCD camera (iXon DV860DC-BV, Andor Technologies, Ireland). Cell cultures were stained (dye concentration 11  $\mu\text{mol/L}$ ) and optically mapped in a perfusion bath with perfusate regulated to 37°C and having the following composition (mmol/L): NaCl 150, KCl 5, CaCl<sub>2</sub> 1.2, MgCl<sub>2</sub> 1, NaHCO<sub>3</sub> 5.8, HEPES 5, and glucose 5 (Hanks Balanced Salt Solution supplemented with Sodium Bicarbonate and HEPES, all from Sigma). Perfusate flow rate was 3.6mL/min. pH was regulated to 7.4. An array of 39 LEDs (Lumina, Mouser Electronics) provided 470nm excitation light, which was further filtered using a 510nm shortpass filter (Edmund Optics) to reduce background fluorescence. A video lens (6mm, f/1.0, Pentax) was used with a series of close-up lenses (Kodak) with a

diopter of +27 to magnify the cell culture. This configuration provided a spatial resolution of 0.28mm per pixel.

### *Measurements*

To achieve steady state conditions, cells were perfused at constant temperature for at least 35 minutes prior to CV measurement. Figure 2 is a diagram of the perfusion apparatus. A clear piece of acrylic was placed on top of the perfusion bath to stabilize the fluid surface for optical recordings. Two unipolar electrodes were extended through in this piece of acrylic to within 400 $\mu$ m of the cell culture to initiate wavefront propagation in either direction through the channel of curved fibers. Pairs of stainless steel meshes on both sides of the perfusion bath grounded stimuli from either corresponding side. 5ms pulse cathodal threshold stimuli were delivered at 350ms intervals, and 16 optical mapping recordings were made per culture, each recording 3 seconds in length. To control for temporal drift in CV, measurements were divided into 4 series of 4 recordings each, and the order of alternating measurements was reversed for each consecutive series (series one consisted of 4 measurements: with  $\kappa$ , against  $\kappa$ , with  $\kappa$ , against  $\kappa$ ; the sequence was reversed for series two: against  $\kappa$ , with  $\kappa$ , against  $\kappa$ , with  $\kappa$ ; and so on).

### *Analysis of Anisotropy*

Compliance of cell orientation to curved scratches was verified by fluorescent actin staining (Alexa Fluor 488, Invitrogen).<sup>16</sup> Anisotropy ratios (longitudinal velocity / transverse velocity) were determined from optical mapping data by tracking propagation

in the longitudinal and transverse directions for wavefronts exiting the curved fiber channel (Figure 1).

### *Data Analysis*

Data were processed in MATLAB (MathWorks Inc.). First, background fluorescence was removed by subtracting a background image from each frame of the dataset. Baseline drift (due to dye bleaching) in temporal data was removed using the MATLAB `detrend()` function. A 60 Hz Fourier bandstop frequency filter with a width of 1.66 Hz was used to minimize 60-cycle noise. Temporal signals across rows of pixels were averaged together (Figure 3), and the resulting signals were 3-point median filtered (MATLAB `medfilt1()`). The maximum derivative of the fluorescence upstroke was used as the activation time for each row of pixels. Each three second recording provided data for 8 or 9 wavefronts traversing the channel of curved fibers. Displacement vs. activation time plots were produced for each wavefront, and the mean activation time for each wavefront was used to align multiple wavefront plots temporally (Figure 3C). Linear regression was used to calculate CV from all the action potentials in each recording. CV values used to determine anisotropy ratios were calculated from multiple wavefronts in the same manner.

### *Statistical Analysis*

The eight CV measurements made in each direction were averaged to give a single TW and a single TA value for each cell culture. A one-sided paired t-test ( $p < 0.05$ ) was used to test the hypothesis that TA propagation is faster than TW propagation. A

group of cultures having the same geometry as in Figure 1, but with straight transverse scratches through the channel, was used as a control to verify that any observed difference in CV was a result of fiber curvature. Control data were scrutinized using a two-sided paired t-test ( $p < 0.05$ ). Averaged measurements were expressed as mean $\pm$ SD.

## Results

A gradient of curvature was produced by the geometry of the substrates used in this experiment (Figure 1), with minimum  $\kappa = 78^\circ/\text{cm}$  and maximum  $\kappa = 333^\circ/\text{cm}$ . The region of curved fibers was 0.57cm long and 0.32cm wide. A range of  $\kappa$  values, rather than a constant  $\kappa$  value throughout the culture, was necessary to maintain a constant spacing between growth directing scratches on the substrate—constant curvature would cause scratch spacings to decrease below  $18\mu\text{m}$  as a function of distance from the centerline of the curved scratch region, while a concentric scratching pattern conserves scratch spacing throughout the region.

Cell culture confluence was assessed using phase contrast microscopy, and nonuniform monolayers were excluded. Cell cultures exhibiting fast ( $< 350\text{ms}$ ) spontaneous rhythms were also excluded, as it would not be possible to initiate wavefronts at the 350ms interval specified by our protocol. 24 curved fiber cell cultures and 8 control cell cultures from three different litters of neonatal rats were used in this experiment. Anisotropy ratios determined for all cultures were  $2.3 \pm 0.3$  ( $n=32$ ). Mean transverse and longitudinal CVs, from the values used in anisotropy ratio calculations, were  $11.0 \pm 3.2$  and  $24.9 \pm 7.0$  cm/s, respectively. Fluorescent actin staining was used to

resolve fiber alignment visually on eight of the cultures after optical mapping data had been recorded (Figure 4).

Paired CV measurements for TA and TW propagation in each culture had a mean difference (TA – TW) of  $0.38 \pm 0.44$  cm/s ( $p=0.00033$ ) (Figure 5). Two of the cell cultures exhibited a  $>1$  cm/s difference between TA and TW propagation velocities, while two other cultures exhibited the reverse of the hypothesized effect (TW propagation was faster than TA propagation in these two samples). Paired measurements of CV in both directions for cultures in the control group had a mean difference of  $0.06 \pm 0.18$  cm/s ( $p=NS$ ).

## **Discussion**

Heterogeneous regions of cardiac tissue are classically defined as localized irregularities in excitability and conduction velocity,<sup>17</sup> and can result from any number of pathologies (congenital factors, such as long-QT or Brugada's syndromes; anatomical deformations, such as hypertrophy or interstitial fibrosis; transient events, including ischemia, stress, electrolytic fluctuations, exposure to drugs, neurotransmitters, or hormones; and basic arrhythmic mechanisms such as reentry, automaticity, triggered activity, cell-to-cell uncoupling and conduction block),<sup>18</sup> or from local variances in temporal factors, such as refractoriness.<sup>19</sup> Arrhythmogenesis typically involves the interplay of several of these conditions. A normal heart rhythm can traverse small obstacles unaffected because a normal wavefront is wide enough to absorb small scale variances; however, faster moving wavefronts, like those emanating from reentrant circuits, have a narrower width and are more susceptible to alteration by tissue

heterogeneities.<sup>20</sup> A simple reentrant waveform, such as a spiral wave, can quickly evolve into a complex fibrillatory pattern upon encountering heterogeneous regions of tissue.<sup>21</sup> Our data provide evidence that fiber curvature can elicit a change in CV; consequently, we conclude that regions of significant fiber curvature can, by definition, constitute tissue heterogeneities. While the resultant effect of this type of heterogeneity is expected to be small (normal wavefronts can propagate across these regions without incident), such changes can synergistically promote arrhythmogenesis in the presence of other factors. For example, curvature effects on propagation may be magnified if high local activation rate causes marginal excitability, and spiral wave drift can be initiated by curved fiber fields,<sup>7</sup> leading to rate acceleration from the Doppler effect.<sup>22</sup> The arrhythmogenic capacities of the papillary and pectinate muscles and their points of insertion are further validated by our findings.

Anisotropy *in vivo* is a product of both cell geometry and nonuniform gap junction distribution. Gap junctions in cultured myocyte preparations do not reproduce such directionally preferential organization, but are instead isotropically distributed.<sup>5,23</sup> However, the anisotropic propagation effects achieved in culture as a result of elongated cellular geometries are functionally similar to the anisotropic effects observed in whole hearts. The growth-directing substrates used in this experiment produced monolayers with an anisotropy ratio ( $2.30 \pm 0.28$ ) that is within the range of anisotropy ratios measured for wavefront propagation in adult ventricular myocardium (1.7 to 3.5).<sup>6</sup>

The effect of fiber curvature on CV can be best understood by considering a differential current element in a curved fiber field (Figure 6). Because the geometry of each cell acts to push current along its longitudinal direction, cells angled away from the

center of the wavefront act to disperse the depolarizing current (as in TW propagation), slowing CV. In the reverse case, when cells are angled towards the center of the wavefront (TA propagation), cellular geometry focuses the depolarizing current.<sup>7</sup> Thus, fiber curvature effects propagation by modulating the effective current load at the leading edge of the wavefront. Similarly, CV changes that result from wavefront curvature in uncurved fiber fields are well documented,<sup>24,25</sup> and operate by the same principle: wavefronts that are concave (with respect to propagation direction) move faster by focusing current toward the center of the wavefront, effectively increasing depolarization charge density; convex wavefronts decentralize depolarizing current, and therefore reduce CV.

In this experiment, the magnitude of the difference in CV for TA versus TW propagation varied significantly from one culture to another. This variability is likely a result of microscopic gaps that occur randomly throughout the cultured monolayers. The presence of these gaps is further confirmed when the transverse and longitudinal CV values from this experiment ( $11.0 \pm 3.2$  cm/s and  $24.9 \pm 7.0$  cm/s, respectively) are compared to the transverse and longitudinal CV measurements made in similarly anisotropic monolayers (anisotropy ratio =  $1.89 \pm 0.38$ ), but on a microscopic scale, by Fast, et al. ( $19.0 \pm 4.3$  cm/s and  $34.6 \pm 4.5$  cm/s, respectively).<sup>6</sup> While microscopic CV measurements can be made in regions selected for optimal confluence, it is highly unlikely that a monolayer of the dimensions used in this experiment would be completely continuous. As the number of such discontinuities increases, the monolayer becomes less of a continuum, and therefore the continuum effect elicited by fiber curvature becomes less significant. Additionally, random dispersion of holes could potentially create

scenarios that alter wavefront morphology for waves entering from one side of the channel but not from the other, possibly explaining the mechanism by which two of the samples exhibited faster TW than TA propagation.

We previously showed that the diffusion tensor, which governs the passive spread of current, can be expanded into three components. One component modulates propagation with respect to wavefront curvature, a second component characterizes fiber curvature effects, and a third component accounts for surface curvature (in 2D).<sup>26</sup> The effect of wavefront curvature has previously been demonstrated experimentally,<sup>27</sup> and this experiment has illustrated the validity of the fiber curvature component. However, the role of surface curvature has yet to be validated experimentally. Computer simulations have also suggested that fiber curvature may play a role in defibrillation shocks.<sup>28</sup>

Curved fiber fields with constant curvature (as opposed to the gradient of curvature produced in this experiment) could be used to determine electrophysiological constants of fiber curvature for use in future simulation studies, and pacing curved fiber fields at higher rates could yield greater insight into the arrhythmogenic potential of curved fiber regions. In the present study, pacing at multiple rates was prohibited by the washout of optical signals after a limited light exposure time (about 50 seconds), and restraining of cultures was not effective. A similar cell culture model could also be used to investigate the effects of three dimensional surface curvature on propagation; computer simulations have shown that surface curvature can induce CV change and spiral drift, even in otherwise homogeneous media.<sup>26</sup>



### Acknowledgements

This project was supported by NIH grants HL64184 and HL67748. We thank Denise Kimbrough and Frank Vance for help with substrate preparation.

### References

1. Sommer JR, Scherer B. Geometry of cell and bundle appositions in cardiac muscle: light microscopy. *Am J Physiol.* 1985;248:H792-803.
2. Hoyt RH, Cohen ML, Saffitz JE. Distribution and three-dimensional structure of intercellular junctions in canine myocardium. *Circ Res.* 1989;64:563-74.
3. Gourdie RG, Green CR, Severs NJ. Gap junction distribution in adult mammalian myocardium revealed by an anti-peptide antibody and laser scanning confocal microscopy. *J Cell Sci.* 1991;99 ( Pt 1):41-55.
4. Spach MS, Kootsey JM, Sloan JD. Active modulation of electrical coupling between cardiac cells of the dog. A mechanism for transient and steady state variations in conduction velocity. *Circ Res.* 1982;51:347-62.
5. Bursac N, Parker KK, Irvanian S, Tung L. Cardiomyocyte cultures with controlled macroscopic anisotropy: a model for functional electrophysiological studies of cardiac muscle. *Circulation research.* 2002;91:e45-54.
6. Fast VG, Kleber AG. Anisotropic conduction in monolayers of neonatal rat heart cells cultured on collagen substrate. *Circ Res.* 1994;75:591-5.
7. Rogers JM, McCulloch AD. Nonuniform muscle fiber orientation causes spiral wave drift in a finite element model of cardiac action potential propagation. *J Cardiovasc Electrophysiol.* 1994;5:496-509.
8. Nielsen PM, Le Grice IJ, Smaill BH, Hunter PJ. Mathematical model of geometry and fibrous structure of the heart. *Am J Physiol.* 1991;260:H1365-78.
9. Vetter FJ, McCulloch AD. Three-dimensional analysis of regional cardiac function: a model of rabbit ventricular anatomy. *Prog Biophys Mol Biol.* 1998;69:157-83.
10. Stevens C, Hunter PJ. Sarcomere length changes in a 3D mathematical model of the pig ventricles. *Prog Biophys Mol Biol.* 2003;82:229-41.

11. Valderrabano M, Lee MH, Ohara T, Lai AC, Fishbein MC, Lin SF, Karagueuzian HS, Chen PS. Dynamics of intramural and transmural reentry during ventricular fibrillation in isolated swine ventricles. *Circ Res*. 2001;88:839-48.
12. Kim YH, Xie F, Yashima M, Wu TJ, Valderrabano M, Lee MH, Ohara T, Voroshilovsky O, Doshi RN, Fishbein MC, Qu Z, Garfinkel A, Weiss JN, Karagueuzian HS, Chen PS. Role of papillary muscle in the generation and maintenance of reentry during ventricular tachycardia and fibrillation in isolated swine right ventricle. *Circulation*. 1999;100:1450-9.
13. Wu TJ, Yashima M, Xie F, Athill CA, Kim YH, Fishbein MC, Qu Z, Garfinkel A, Weiss JN, Karagueuzian HS, Chen PS. Role of pectinate muscle bundles in the generation and maintenance of intra-atrial reentry: potential implications for the mechanism of conversion between atrial fibrillation and atrial flutter. *Circ Res*. 1998;83:448-62.
14. Gray RA, Pertsov AM, Jalife J. Incomplete reentry and epicardial breakthrough patterns during atrial fibrillation in the sheep heart. *Circulation*. 1996;94:2649-61.
15. Rohr S, Scholly DM, Kleber AG. Patterned growth of neonatal rat heart cells in culture. Morphological and electrophysiological characterization. *Circ Res*. 1991;68:114-30.
16. Barak LS, Yocum RR, Nothnagel EA, Webb WW. Fluorescence staining of the actin cytoskeleton in living cells with 7-nitrobenz-2-oxa-1,3-diazole-phalloidin. *Proc Natl Acad Sci U S A*. 1980;77:980-4.
17. Moe GK, Rheinboldt WC, Abildskov JA. A Computer Model of Atrial Fibrillation. *Am Heart J*. 1964;67:200-20.
18. Zipes DP, Wellens HJ. Sudden cardiac death. *Circulation*. 1998;98:2334-51.
19. Winfree AT. *When Time Breaks Down*. New Jersey: Princeton University Press; 1987.
20. Bub G, Shrier A. Propagation through heterogeneous substrates in simple excitable media models. *Chaos*. 2002;12:747-753.
21. Fenton FH, Cherry EM, Hastings HM, Evans SJ. Multiple mechanisms of spiral wave breakup in a model of cardiac electrical activity. *Chaos*. 2002;12:852-892.
22. Perez-Munuzuri V, Aliev R, Vasiev B, Perez-Villar V, Krinsky VI. Super-spiral structures in an excitable medium. 1991;353:740-742.
23. Fast VG, Kleber AG. Microscopic conduction in cultured strands of neonatal rat heart cells measured with voltage-sensitive dyes. *Circ Res*. 1993;73:914-25.

24. Kay MW, Gray RA. Measuring curvature and velocity vector fields for waves of cardiac excitation in 2-D media. *IEEE Trans Biomed Eng.* 2005;52:50-63.
25. Fast VG, Kleber AG. Role of wavefront curvature in propagation of cardiac impulse. *Cardiovasc Res.* 1997;33:258-71.
26. Rogers JM. Wave front fragmentation due to ventricular geometry in a model of the rabbit heart. *Chaos.* 2002;12:779-787.
27. Knisley SB, Hill BC. Effects of bipolar point and line stimulation in anisotropic rabbit epicardium: assessment of the critical radius of curvature for longitudinal block. *Biomedical Engineering, IEEE Transactions on.* 1995;42:957-966.
28. Trayanova N, Skouibine K. Modeling defibrillation: effects of fiber curvature. *J Electrocardiol.* 1998;31 Suppl:23-9.

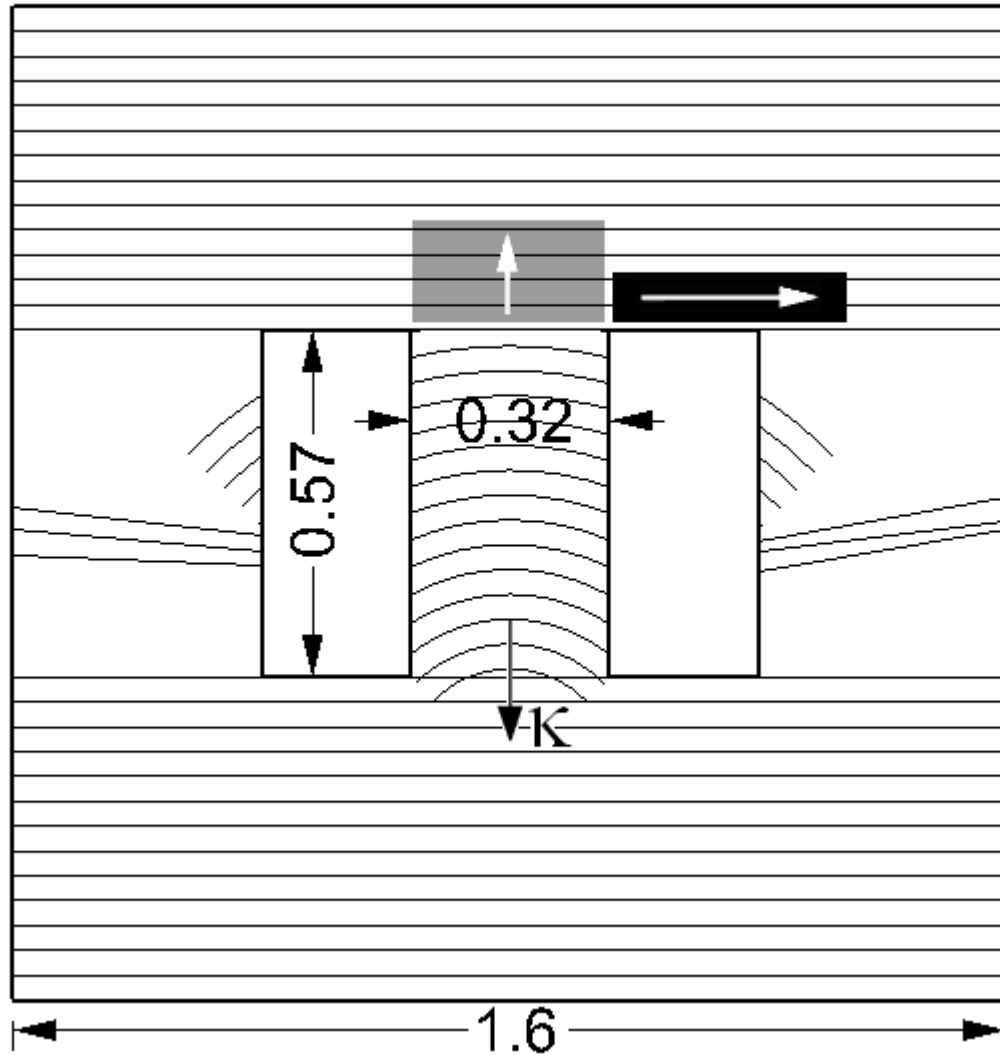


Figure 1. Geometry of growth directing substrates. Isotropic regions on both sides of the culture were scratched three times with a scalpel to prevent wavefront reentry. Shaded boxes represent regions of measurement of longitudinal (black) and transverse (gray) velocities used in anisotropy ratio calculations. White arrows denote propagation direction in those measurements.  $\kappa$  vector not drawn to scale.

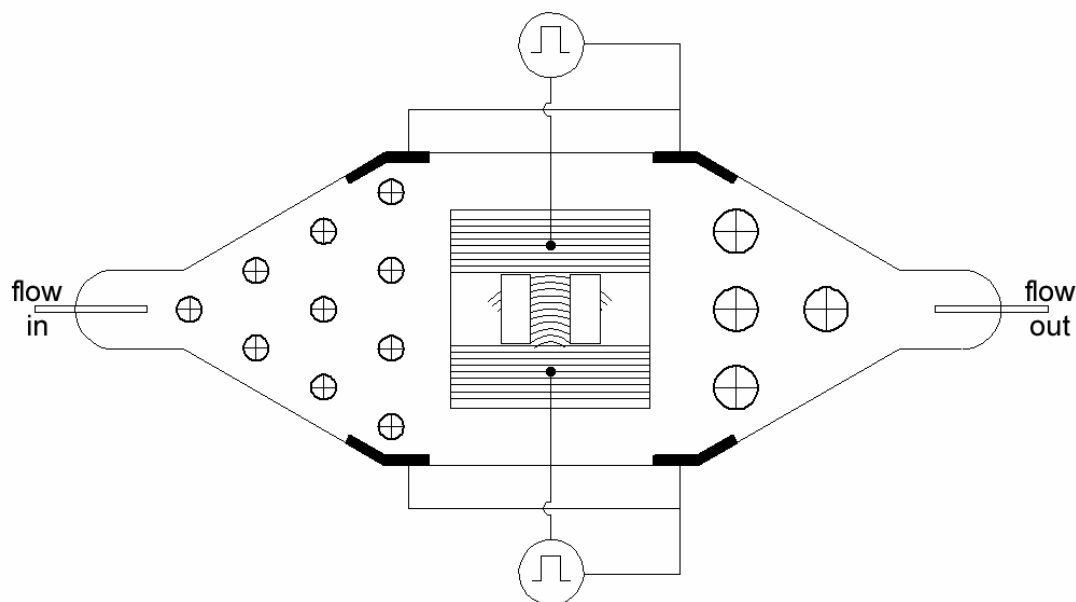


Figure 2. Geometry of perfusion bath with electrodes. Arrays of circles on either side of the cell culture represent cylindrical obstacles that encouraged a smooth perfusate flow profile. All electrodes shown in black. Two grounding electrodes were paired with each unipole to ground stimuli from either side of the cell culture.

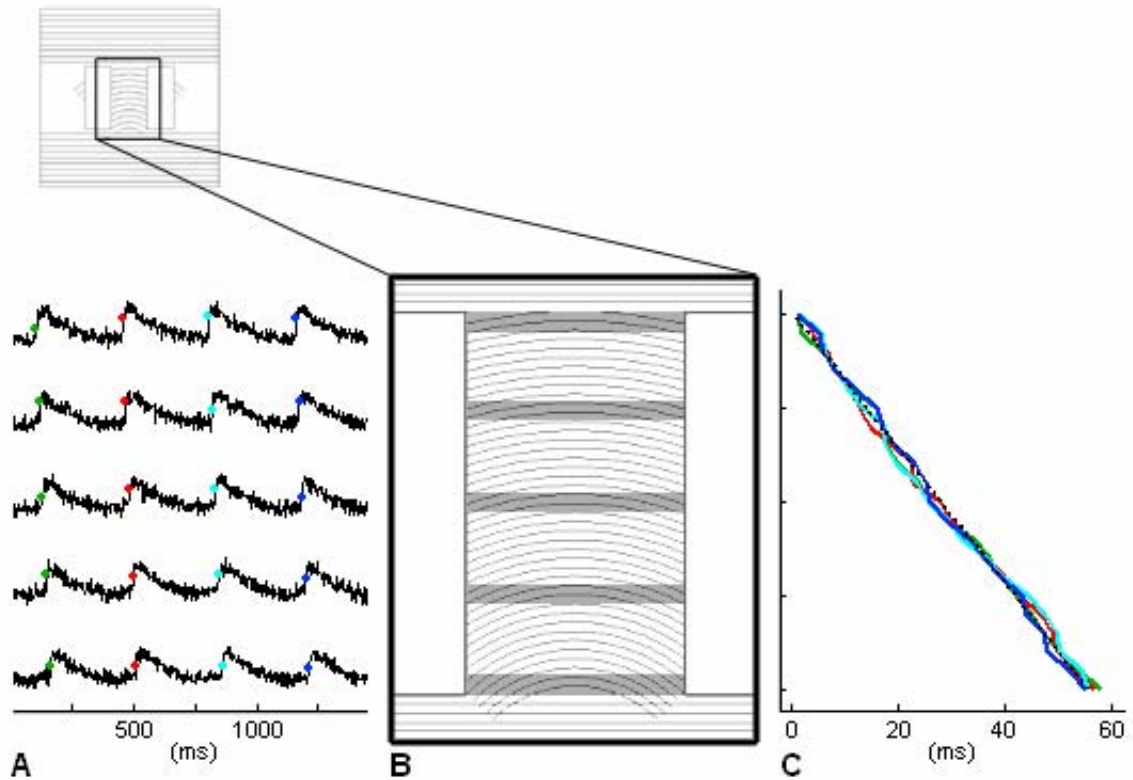


Figure 3. Method for conduction velocity calculation. A, Activation times, determined by the maximum derivative of the upstroke for each depolarization, were recorded for each wavefront by averaging across each row of pixels in the channel. B, Channel of curved fibers. Gray regions denote single rows of pixels corresponding to data displayed in A. Channel is 0.57cm long. C, Displacement vs. time for all wavefronts, showing data from all rows of pixels. Linear regression is shown as a black dotted line. Like colors correspond to the same wavefronts in A and C.

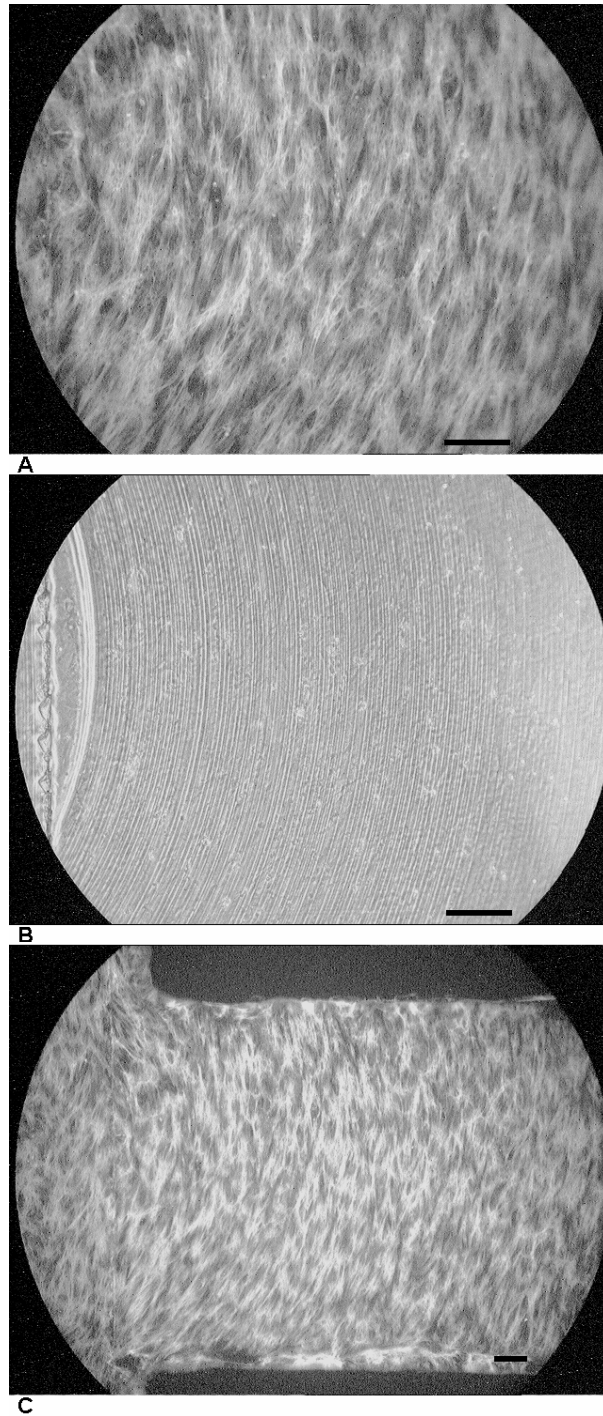


Figure 4. A, Myofibril curvature as resolved by fluorescent actin filament staining. B, phase contrast image showing scratches in the same region. C, fluorescence image of the same culture at lower magnification. Bars = 200 $\mu$ m.

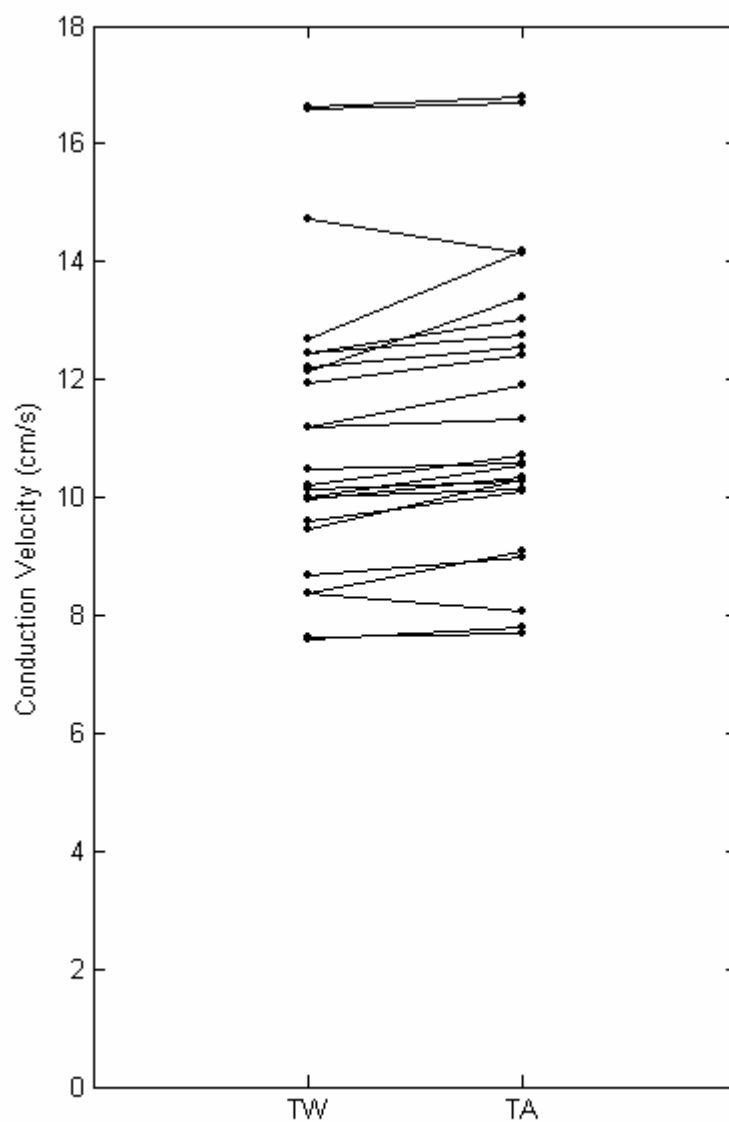


Figure 5. Average conduction velocities for all curved fiber samples. Each line represents all TW and TA measurements from one cell culture.



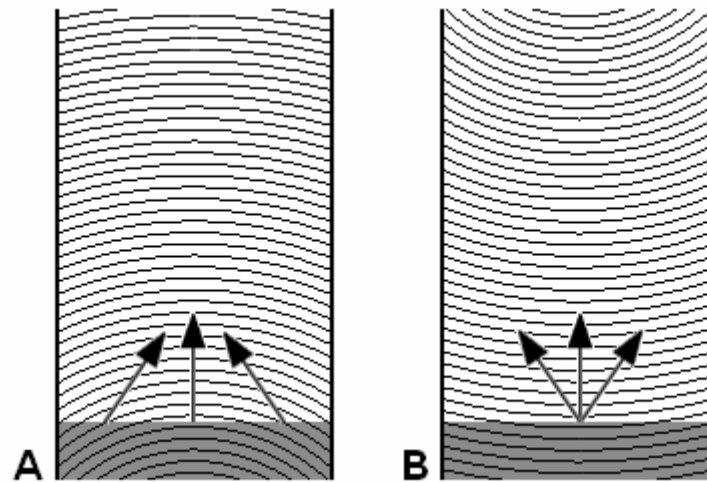


Figure 6. Two dimensional propagation across curved fibers of anisotropic cells. Gray regions denote depolarized cells. Arrows indicate dominant directions for the anisotropic spread of depolarizing current. Wavefronts are moving from the bottom to the top in both panels. A, TA propagation. Fiber curvature increases CV by increasing current density in the direction of propagation. B, TW propagation. Fiber curvature causes decentralization of the depolarizing current, slowing CV.

## CONCLUSIONS

The goal of this project was to experimentally verify the role played by fiber curvature in wavefront propagation. This project involved creating a growth-directing substrate to produce controlled fiber curvature in anisotropic monolayers of cells. Conduction velocities were measured for waves propagating transversely with (TW) and transversely against (TA) the direction of fiber curvature, as defined by the curvature vector  $\kappa$ . A paired t-test ( $p < 0.05$ ) was used to determine the significance of the CV change produced by alternating the propagation direction with respect to the curvature vector. These data were compared with control, consisting of CV measurements for propagation in both transverse directions in uncurved fiber fields.

A difference in CV of  $0.38 \pm 0.44$  cm/s (TA CV – TW CV) was measured when propagation direction was reversed with respect to  $\kappa$ , and this difference was found to be statistically significant ( $p = 0.00033$ ) ( $n = 24$ ). The CV difference measured when propagation direction was alternated in the control group ( $n = 8$ ) was  $0.06 \pm 0.18$  cm/s ( $p = \text{NS}$ ). The effect of fiber curvature on wavefront propagation, as previously shown in computer simulations,<sup>8</sup> was experimentally confirmed by these findings. These results further illustrated the arrhythmogenic potential of highly curved regions in the myocardium (i.e., papillary and pectinate muscles). Further work is needed to determine electrophysiological constants that relate CV change to variable degrees of curvature and variable pacing rates.

## REFERENCES

1. Fox CS, Evans JC, Larson MG, Kannel WB, Levy D. Temporal trends in coronary heart disease mortality and sudden cardiac death from 1950 to 1999: the Framingham Heart Study. *Circulation*. 2004;110:522-7.
2. Zipes DP, Wellens HJ. Sudden cardiac death. *Circulation*. 1998;98:2334-51.
3. Huikuri HV, Castellanos A, Myerburg RJ. Sudden death due to cardiac arrhythmias. *N Engl J Med*. 2001;345:1473-82.
4. Fenton FH, Cherry EM, Hastings HM, Evans SJ. Multiple mechanisms of spiral wave breakup in a model of cardiac electrical activity. *Chaos*. 2002;12:852-892.
5. Bub G, Shrier A. Propagation through heterogeneous substrates in simple excitable media models. *Chaos*. 2002;12:747-753.
6. Moe GK, Rheinboldt WC, Abildskov JA. A Computer Model of Atrial Fibrillation. *Am Heart J*. 1964;67:200-20.
7. Winfree AT. *When Time Breaks Down*. New Jersey: Princeton University Press; 1987.
8. Rogers JM, McCulloch AD. Nonuniform muscle fiber orientation causes spiral wave drift in a finite element model of cardiac action potential propagation. *J Cardiovasc Electrophysiol*. 1994;5:496-509.
9. Rogers JM. Wave front fragmentation due to ventricular geometry in a model of the rabbit heart. *Chaos*. 2002;12:779-787.
10. Skinner GS, Swinney HL. Periodic to quasiperiodic transition of chemical spiral rotation. *Physica D: Nonlinear Phenomena*. 1991;48:1-16.
11. Fast VG, Pertsov AM. [Drift of vortex in the myocardium]. *Biofizika*. 1990;35:478-82.
12. Perez-Munuzuri V, Aliev R, Vasiev B, Perez-Villar V, Krinsky VI. Super-spiral structures in an excitable medium. 1991;353:740-742.

13. Nielsen PM, Le Grice IJ, Smaill BH, Hunter PJ. Mathematical model of geometry and fibrous structure of the heart. *Am J Physiol.* 1991;260:H1365-78.
14. Vetter FJ, McCulloch AD. Three-dimensional analysis of regional cardiac function: a model of rabbit ventricular anatomy. *Prog Biophys Mol Biol.* 1998;69:157-83.
15. Stevens C, Hunter PJ. Sarcomere length changes in a 3D mathematical model of the pig ventricles. *Prog Biophys Mol Biol.* 2003;82:229-41.
16. Gray RA, Pertsov AM, Jalife J. Incomplete reentry and epicardial breakthrough patterns during atrial fibrillation in the sheep heart. *Circulation.* 1996;94:2649-61.
17. Wu TJ, Yashima M, Xie F, Athill CA, Kim YH, Fishbein MC, Qu Z, Garfinkel A, Weiss JN, Karagueuzian HS, Chen PS. Role of pectinate muscle bundles in the generation and maintenance of intra-atrial reentry: potential implications for the mechanism of conversion between atrial fibrillation and atrial flutter. *Circ Res.* 1998;83:448-62.
18. Valderrabano M, Lee MH, Ohara T, Lai AC, Fishbein MC, Lin SF, Karagueuzian HS, Chen PS. Dynamics of intramural and transmural reentry during ventricular fibrillation in isolated swine ventricles. *Circ Res.* 2001;88:839-48.
19. Kim YH, Xie F, Yashima M, Wu TJ, Valderrabano M, Lee MH, Ohara T, Voroshilovsky O, Doshi RN, Fishbein MC, Qu Z, Garfinkel A, Weiss JN, Karagueuzian HS, Chen PS. Role of papillary muscle in the generation and maintenance of reentry during ventricular tachycardia and fibrillation in isolated swine right ventricle. *Circulation.* 1999;100:1450-9.
20. Victor S, Nayak VM. Variations in the papillary muscles of the normal mitral valve and their surgical relevance. *J Card Surg.* 1995;10:597-607.
21. Fast VG, Cheek ER. Optical mapping of arrhythmias induced by strong electrical shocks in myocyte cultures. *Circ Res.* 2002;90:664-70.
22. Gillis AM, Fast VG, Rohr S, Kleber AG. Mechanism of ventricular defibrillation. The role of tissue geometry in the changes in transmembrane potential in patterned myocyte cultures. *Circulation.* 2000;101:2438-45.
23. Bian W, Tung L. Structure-related initiation of reentry by rapid pacing in monolayers of cardiac cells. *Circ Res.* 2006;98:e29-38.

24. Fast VG, Kleber AG. Cardiac tissue geometry as a determinant of unidirectional conduction block: assessment of microscopic excitation spread by optical mapping in patterned cell cultures and in a computer model. *Cardiovasc Res.* 1995;29:697-707.
25. Bursac N, Parker KK, Iravanian S, Tung L. Cardiomyocyte cultures with controlled macroscopic anisotropy: a model for functional electrophysiological studies of cardiac muscle. *Circ Res.* 2002;91:e45-54.
26. Fast VG, Kleber AG. Anisotropic conduction in monolayers of neonatal rat heart cells cultured on collagen substrate. *Circ Res.* 1994;75:591-5.
27. Barak LS, Yocum RR, Nothnagel EA, Webb WW. Fluorescence staining of the actin cytoskeleton in living cells with 7-nitrobenz-2-oxa-1,3-diazole-phalloidin. *Proc Natl Acad Sci U S A.* 1980;77:980-4.


## APPENDIX

### IACUC ANIMAL USE APPROVAL FORM

**NOTICE OF APPROVAL**

**DATE:** October 3, 2006

**TO:** Jack M. Rogers, Ph.D.  
VH-B140 0019  
FAX: 975-4720

**FROM:**   
Judith A. Kapp, Ph.D., Chair  
Institutional Animal Care and Use Committee

**SUBJECT:** Title: Mechanisms for Maintenance of Ventricular Fibrillation  
Sponsor: NIH  
Animal Project Number: 060906873

On September 28, 2006, the University of Alabama at Birmingham Institutional Animal Care and Use Committee (IACUC) reviewed the animal use proposed in the above referenced application. It approved the use of the following species and numbers of animals:

Species	Use Category	Number in Category
Pigs	B	28
Rats	A	30

Animal use is scheduled for review one year from September 2006. Approval from the IACUC must be obtained before implementing any changes or modifications in the approved animal use.

Please keep this record for your files, and forward the attached letter to the appropriate granting agency.

Refer to Animal Protocol Number (APN) 060906873 when ordering animals or in any correspondence with the IACUC or Animal Resources Program (ARP) offices regarding this study. If you have concerns or questions regarding this notice, please call the IACUC office at 934-7692.

**Institutional Animal Care and Use Committee**  
B10 Volker Hall  
1670 University Boulevard  
205.934.1294  
FAX 205.975.7886

Mailing Address:  
VH B10  
1530 3RD AVE S  
BIRMINGHAM AL 35294-0019